Catal Lett (2015) 145:1251–1261
DOI 10.1007/s10562-015-1522-7

Sol–Gel Preparation of Samaria Catalysts for the Oxidative Coupling of Methane

Björn Neumann[1] · Trenton W. Elkins[2] · Alexander E. Gash[3] · Helena Hagelin-Weaver[2] · Marcus Bäumer[1]

Received: 4 November 2014 / Accepted: 17 March 2015 / Published online: 6 May 2015

Abstract A new sol–gel synthesis route for alumina–samaria mixed aero- and xerogel catalysts based on the so-called epoxide addition method and the use of these systems as catalysts for the oxidative coupling of methane (OCM) is reported. As precursors simple chloride or nitrate salts can be used. The mesoporous materials are X-ray amorphous even after calcination to 800 °C and show an intimate mixing of Al and Sm on the nanoscale. In the case of the xerogels derived from chlorides, C_2 yields comparable to pure samaria can be achieved under OCM reaction conditions with 100 % O_2 conversion. Even at lower O_2 conversions the activity of the xerogel is competitive with a pure samaria reference catalyst taking the lower samaria content of 20 % into account. Accordingly, the approach is suitable to reduce the costs associated with the rare earth oxide. In addition to the preparation of aerogel and xerogel particles, the presented synthesis also allows the fabrication of xerogel films which can be coated on a suitable (monolithic) support. First results of such films are presented.

Graphical Abstract

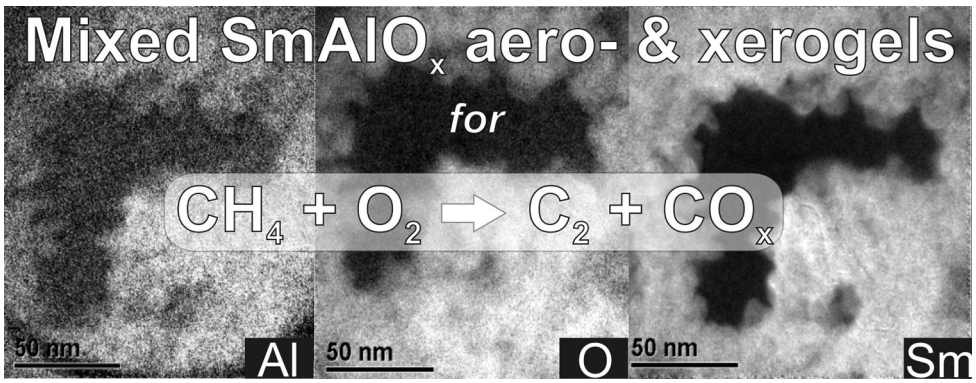

Keywords Oxidative methane coupling · Sol–gel chemistry · Rare earth oxide catalyst

Electronic supplementary material The online version of this article (doi:10.1007/s10562-015-1522-7) contains supplementary material, which is available to authorized users.

✉ Helena Hagelin-Weaver
hweaver@che.ufl.edu

✉ Marcus Bäumer
mbaeumer@uni-bremen.de

[1] Institute of Applied and Physical Chemistry & Center for Environmental Research and Sustainable Technology, University of Bremen, Leobener Str., 28359 Bremen, Germany

[2] Department of Chemical Engineering, University of Florida, Gainesville, FL 32611, USA

[3] Chemistry and Chemical Engineering Division, Chemistry and Materials Science Directorate, Lawrence Livermore National Laboratory, Livermore, CA 94550, USA

1 Introduction

Methane is the major component of natural gas and—as it is more abundant than crude oil—the fossil fuel that will be available longest. In addition, it can also be produced from biodegradable materials commonly known as "bio gas" and is thus expected to play a central role as a renewable resource as well [1]. Most of the methane—independent of its source—is still used for the generation of heat and electricity [2]. Yet, its activation and conversion into higher hydrocarbons would open valuable pathways to use methane also for the production of chemicals which today are obtained from crude-oil. The oxidative coupling of methane (OCM) is one of the options in this respect and has thus attracted renewed interest recently [2]. It allows the conversion of methane into ethane and ethylene along with CO and CO_2 formed as undesired by-products. A major aim of OCM catalyst development is suppressing total oxidation and increasing the C_{2+} yield, i.e. the yield of C_2H_6, C_2H_4 and higher hydrocarbon products. Here, basic oxides have been shown to be good catalysts for the process typically carried out at temperatures between 600 and 800 °C [3, 4]. Two of the most intensively studied systems in this respect are lithium doped magnesia which was pioneered by Lunsford and coworkers [5], and Mn–Na_2WO_4/SiO_2 which was first discovered by Li [6]. While Mn–Na_2WO_4/SiO_2 is considered to be the state-of-the-art OCM catalyst, it is a very complex system, and the nature of the active sites is still under debate [7]. Li/MgO is receiving less attention in recent literature as it is associated with rapid deactivation due to Li removal during reaction [8, 9]. Other catalysts commonly used for the OCM reaction are doped and undoped rare earth oxides (REOs) [7]. Amongst these, samaria is among the most active single component catalysts for the oxidative coupling of methane [10, 11]. C_{2+} yields of 12 % (with a range from 6 to 12 %) have been reported under certain conditions over pure Sm_2O_3 and its activity and selectivity can be further increased by alkali metal doping [12]. Samaria is therefore a good choice for studying the effects of different synthesis techniques on OCM catalysts.

REOs are not rare when comparing their abundance in the earth crust with other catalytically employed elements, in particular noble metals. However, their prices have been rising steadily for several years. In order to minimize the use of the expensive samaria, it can be deposited on an inert, less expensive oxide or embedded in a suitable matrix. For OCM, various preparation methods of samaria catalysts, including incipient wetness impregnation (IWI) and micro emulsion, have already been reported [13–15].

In comparison to these classical methods, sol–gel techniques offer a large toolbox to control and tune parameters which are important for the catalytic performance, such as composition (including matrix embedding and doping) and porosity [16–18]. Among the sol–gel methods, the so-called epoxide addition method (EAM) provides a particularly convenient route, allowing the use of simple metal salts, such as metal chlorides or nitrates as precursors (instead of expensive and sometimes very reactive alkoxides) for the synthesis [19]. The resulting materials are aero- and xerogels (after supercritical drying or drying in air, respectively), which are often obtained in a monolithic form but can be crushed to a powder of suitable grain size. Interestingly, however, EAM is not limited to the preparation of such aero- or xerogels, but is also suitable for the fabrication of coatings [20].

Such coatings are of particular interest in combination with monolithic reactor concepts proven to be beneficial for the performance of OCM catalysts, since e.g. hot spot formation in the reactor can be avoided [21–23]. Lunsford and coworkers were the first to test honeycomb structures, but found no significant advantage [21]. In a previous publication, we showed that ceramic foams as an alternative do provide advantages in terms of C_2 yields as a result of a turbulent flow pattern in comparison to the laminar flow in honeycomb structures [24]. Yet, the synthesis technique used there (a polyurethane foaming technique) involved the preparation of bulk samaria monoliths and is not economically attractive because of the need to use large amounts of the expensive material.

Therefore, we pursued two approaches based on the EAM in the present study to circumvent this problem. First, we extended the synthesis from pure samaria aero- and xerogels, described in a previous publication to mixed alumina/samaria systems with samaria contents of only at 20 %. While alumina is a commonly used catalyst support, it is not typically used in OCM due to its high surface area and acidic properties [25]. Basic supports, such as MgO or CaO, are more common in OCM as they result in higher C_{2+} selectivities than acidic alumina supports [26, 27]. Nevertheless, alumina supports have shown promise in the OCM reaction [13]. We show that the mixed aero- and xerogels indeed exhibit C_2 yields which are competitive to the pure samaria systems. Second, we tested the process for the application of coatings on an oxidic substrate, opening the option to deposit just a thin layer of the catalyst on the surface of suitable ceramic foam of a cheap material, such as alumina or silica [28].

2 Experimental

2.1 Sol–Gel Preparation and Reference Catalyst Synthesis

Alumina stabilized samaria aerogels were prepared expanding the epoxide addition sol–gel method established

by Gash et al. [19]. All reactants were reagent grade or better and used as received. The alumina/samaria precursor mixture consisted either of aluminum chloride hexahydrate (Alfa) and samarium (III) chloride hexahydrate (Chempur, Karlsruhe, Germany) or of aluminium nitrate nonahydrate (Alfa) and samarium nitrate hexahydrate (Chempur, Karlsruhe, Germany) at 80 and 20 mol% respectively. For a typical batch 2.4 mmol of the alumina precursor and 0.6 mmol of samarium precursor were dissolved in 5 g of absolute ethanol (Roth, Germany). Propylene oxide (Sigma-Aldrich) was used as the gelation agent. The molar ratio of metal salt to gelling agent was 0.1.

The sols were placed in cylindrical PE vials, covered and allowed to gel and age for at least 24 h under ambient conditions. The resulting gels were then immersed in a bath of absolute ethanol where they were washed daily over a span of 3 days by changing the ethanol. These alcogels were either processed to aerogels in a BALTEC supercritical point drier or dried under ambient conditions leading to xerogels. In the former case the alcohol in the gel pores was exchanged for liquid CO_2 for 3 days at about 10 °C, after which the temperature of the vessel was ramped up to about 45 °C while not exceeding a pressure of ~100 bar. The vessel was then depressurized at a rate of about 7 bar/h. The resulting aerogels and xerogels were calcined at 800 °C for 4 h.

For the coating experiments the same approach was used as for the sol preparation. Before the gel point was reached, the solution was used to drop coat a piece of quartz glass which was pretreated with acetone.

Two reference catalysts were prepared by simply calcining samarium nitrate hexahydrate, or a mixture of samarium nitrate hexahydrate and aluminium nitrate nonahydrate, in air at 800 °C for 4 h. The third reference catalyst was prepared by incipient wetness impregnation of an aqueous solution of samarium nitrate onto an alumina support (Alfa Aesar), as previously described [13].

2.2 N_2 Adsorption

Nitrogen adsorption isotherms were measured at 77 K using a QuadraSorb sorption analyzer (Quantachrome Instrument Corp.). All samples were degassed for 20 h at 120 °C prior to sorption experiments. Pore size distributions were obtained from the measured N_2 desorption isotherms by applying the Barrett-Joyner-Halenda (BJH) method.

2.3 Transmission Electron Microscopy and Related Techniques

Transmission electron microscopy was performed using an FEI Tecnai F20 S-TWIN microscope. The microscope was operated at an accelerating voltage of 200 kV. TEM and energy-filtered images (EF-TEM) were recorded with a slow-scan CCD camera with an integrated Gatan Image Filter Model 2001. EF-TEM maps of Sm, Al, O were acquired on the basis of the three-window method at ionization edges of the elements. For the preparation of the TEM grids, a small amount of each sample was suspended in acetone and ultrasonicated for at least 5 min. Afterwards, a droplet (25 μL) was placed on carbon-coated copper grids. To estimate the average ligament size of each gel, 150 ligaments were measured.

2.4 Powder X-Ray Diffraction

Powder X-ray diffraction (PXRD) data was collected on aerogel and xerogel samples using an PANalytical XPERT MPD Pro 1 diffractometer utilizing Cu $K_{\alpha 1,2}$ radiation. Samples were mounted on a standard sample holder.

2.5 Catalytic Experiments

The samaria based aerogels and xerogels were probed for activity under OCM conditions. The reactor system has been previously described in detail [13]. This system consists of a quartz tube reactor with inner diameters (IDs) of either 10 or 4 mm, dependent on the experiment (see below). Product monitoring was accomplished with an online gas chromatograph (GC) equipped with two columns and two detectors in series. The thermal conductivity detector (TCD) was typically used for product monitoring, but a flame ionization detector (FID) preceeded by a methanizer to convert all CO and CO_2 to CH_4 was used when needed to increase the sensitivity to CO, CO_2 and C_{2+} products. The gels were sieved to a particle size range between 180 and 250 microns prior to loading the reactor. The samples were outgassed under a N_2 flow at 105 °C overnight before exposure to OCM conditions. In most of the experiments, the 10-mm ID reactor was used with 400 mg catalyst and a total flow rate of 120 sccm to facilitate comparisons with our previous study [24]. Nitrogen (N_2) was used as an inert internal standard for the GC, and it was fed to the reactor at a constant flow rate of 23.2 sccm. Three CH_4:O_2 ratios were investigated; 9:1, 7:1, 4:1, together with two reaction temperatures; 740 and 800 °C for each catalyst. In all cases (not shown), the 4:1 CH_4:O_2 ratio resulted in the highest C_2 yield, since the conversion increased significantly with decreasing CH_4:O_2 ratio, while the C_2 selectivity was fairly constant. Methane conversions measured were reproducible within ±1.0 %. Furthermore, for all alumina-containing catalysts, a reaction temperature of 800 °C yielded more C_2 products than at 740 °C. Therefore, only data for a CH_4:O_2 ratio of 4:1 and a reaction temperature of 800 °C are presented.

For the flow rate studies (400 mg catalyst in the 10 mm ID reactor), a fresh catalyst was loaded into the reactor and the products were monitored after the reactor temperature reached 800 °C starting at 120 sccm, and then incrementally increasing the flow rate. A few experiments were conducted with smaller amounts of catalyst (75, 50 and 10 mg) in a smaller diameter reactor (4-mm ID). Again, for each experiment, a fresh catalyst was loaded and the flow rate was increased once the reactor reached 800 °C.

3 Results and Discussion

Following a strategy for the preparation of pure REO aero- and xerogels based on EAM published previously, we investigated the synthesis of mixed samaria-alumina aero- and xerogels. We performed a careful characterization of these materials, and subsequently tested their catalytic performance with respect to the oxidative coupling of methane. As a proof of principle, we finally explored the suitability of EAM for the preparation of thin layers (catalytic coatings) of the investigated materials. The results are described in the following sections.

3.1 Synthesis

A major advantage of the EAM in comparison to other sol–gel approaches is the option to use "simple" metal salts as precursors. In the present case, we employed samarium and aluminum nitrate or chloride, respectively, to prepare the mixed systems. At room temperature gel formation took place within 20 min after the addition of propylene oxide to the solutions. After drying in air and calcination at 800 °C, the resulting xerogels exhibited a light yellow color. Aerogels obtained by supercritical drying (also followed by calcination) were close to white in color.

In our former work we showed that pure samaria gels can neither be obtained from samarium nitrate nor samarium chloride. In the former case no gelation occurred, while in the latter case up to 10 wt% of crystalline samarium oxychloride was formed [28]. The mixed gel, however, did not show any oxychloride phases in XRD. Checking the chloride-derived sample by X-ray photo electron spectroscopy (XPS) and chemical analysis revealed that chloride residues are present in the samples prior to the calcination. However, after the heat treatment at 800 °C, chlorine could neither be detected on the surface, probed by XPS, nor in the bulk probed by (a) EDX and (b) dissolving the sample in HNO_3 and performing a silver-chloride test. Apparently, the addition of aluminum renders the synthesis more robust and, at the same time, more flexible with respect to the precursor allowing the formation of pure oxide xero- and aerogels from chlorides and nitrates without detectable contaminations (in particular no oxychloride formation).

3.2 Characterization

3.2.1 Transmission Electron Microscopy

Figure 1 shows the TE micrographs of the resulting aero- and xerogel after calcination. Aerogels show a typical open cell morphology as was also observed for pure alumina aeorgels previously [16]. In comparison to the aerogels, the xerogels have a denser appearance, suggesting a lower porosity. The mean diameter of the ligaments increases from $\sim$5 nm for the aerogels (nitrate < chloride) to $\sim$10 nm for the xerogels (again nitrate < chloride). For pure alumina aerogels, Baumann et al. observed different morphologies when using either chloride or nitrate salts as precursors for the aerogels. Their gels showed fibrous (chloride) or more particulate (nitrate) structures, respectively. The different appearance of the resulting gels was traced back to changes in the ratio between reaction rates of hydrolysis and (poly)-condensation which—although being small—have a large influence on the gel morphology [16]. In our case we introduced an additional ion to the system. The samarium ions may influence the reaction rates of hydrolysis and condensation so that the structural differences between nitrate or chloride samples become less pronounced in comparision to pure alumina gels.

Figure 2 displays representative EF-TEM images showing the spatial distribution of oxygen, aluminum and samarium in these samples. Within the resolution of the experiment, the distribution of these elements is homogenous; even after calcination no separated alumina and samaria areas form.

3.2.2 Nitrogen Adsorption

The observations made by TEM are supported by the nitrogen adsorption measurements (see supporting information). The mixed aerogels show higher specific surface areas—up to a factor of two for the chloride derived samples—compared with their xerogel counterparts (Table 1). Pure alumina aero-and xerogels always show a higher SSA in comparison to the mixed systems. Also here, the surface area of the xerogels is smaller than the surface area of the aerogels for the pure alumina. Comparing the pure alumina and the mixed systems, it needs to be considered that the addition of considerable amounts of samarium leads to an increase of the molar mass of the materials (1 mol pure Al_2O_3 and 0.2 mol Sm_2O_3 + 0.8 - mol Al_2O_3 are compared). The ratio of the molar masses of the pure and the mixed system is close to 1.5 so that of course the SSA—by its definition—changes; the structural

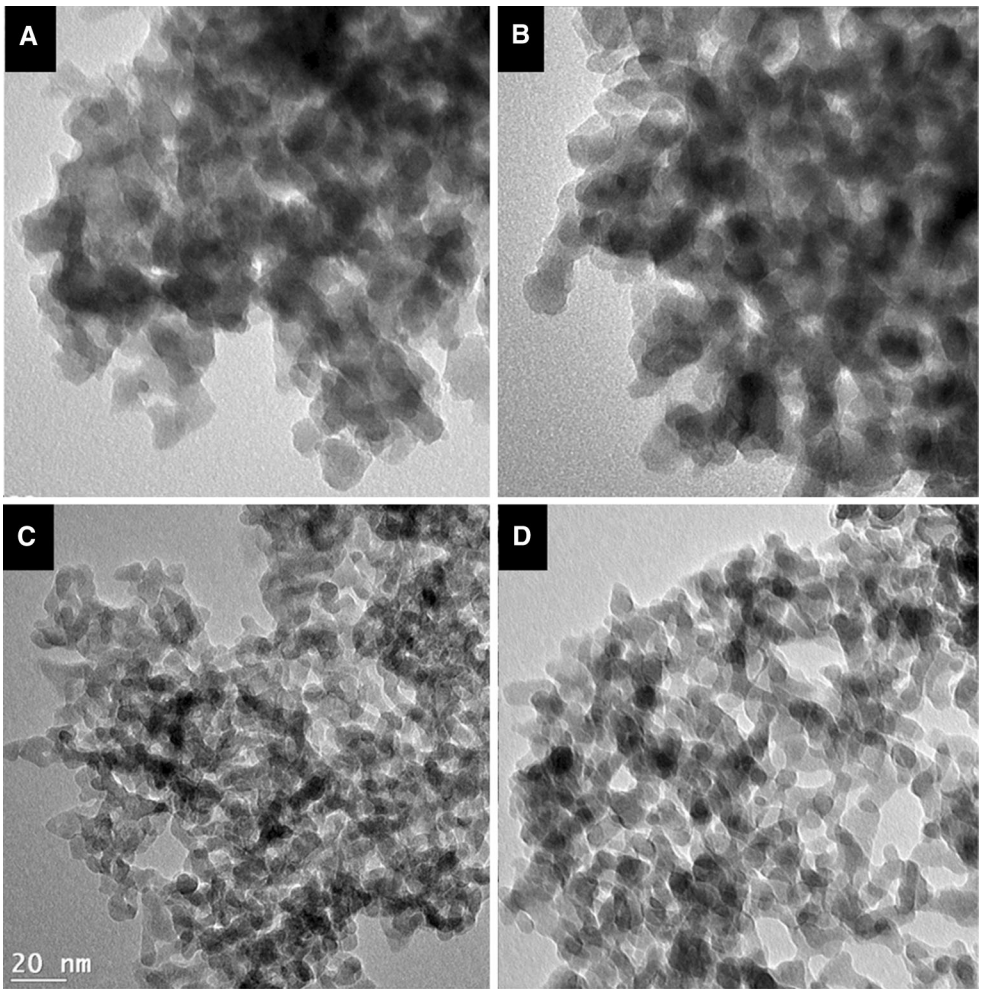

Fig. 1 Transmission electron micrographs of Al_2O_3/Sm_2O_3 sol–gel derived materials (*all with the same magnification*). **a** xerogel (nitrate), **b** xerogel (chloride), **c** aerogel (nitrate), and **d** aerogel (chloride). All sol–gel materials were calcined in air at 800 °C for 4 h before collecting the images

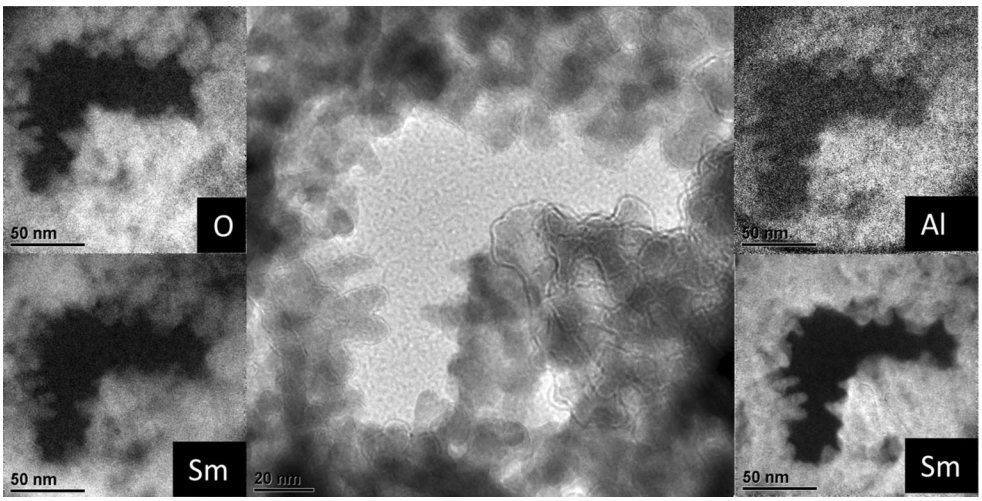

Fig. 2 Energy filtered transmission electron microscopy (EF-TEM) images of the mixed aluminium samarium aerogel derived from nitrates. On the investigated length scale the distribution of the elements Sm, Al and O is homogenous. The two Sm maps were collected at two different Sm edges

Table 1 The specific surface area, pore volume, and the maximum of the pore size distribution (BJH) for the sol–gel derived samaria on alumina samples

Notation	BET surface area (m^2/g)	Pore volume[a] (cm^3/g)	Max. pore size distribution[a] (nm)
Sm_2O_3/Al_2O_3 AG Cl	119	1.80	53
Sm_2O_3/Al_2O_3 XG Cl	64	0.42	19
Sm_2O_3/Al_2O_3 AG NO_3	164	**	**
Sm_2O_3/Al_2O_3 XG NO_3	117	0.16	4

[a] Calculated using Barrett-Joyner-Halenda (BJH) method, for calcined catalysts only (aerogel [AG] and xerogel [XG] samples prepared using nitrate [NO_3] or chloride [Cl] precursors)

** The BJH analysis did not give reliable values due to the macro-pores of this catalyst

differences are thus less severe as it would be the case when comparing two materials of the same composition.

A BJH analysis of the desorption branches of the nitrogen adsorption isotherm reveals again what TEM already suggested, namely that the maximum of the pore size distribution of samaria-alumina xerogel derived from the chlorides is smaller by a factor of 2.5 compared to the respective aerogels. In addition, the aerogel showed a broader pore size distribution with pores in the range of 20 nm to larger than 50 nm. For the nitrate derived sample a BJH analysis of the aerogel was not possible. The adsorption isotherm did not show hysteresis during desorption of nitrogen indicating that most of the pore volume is outside the mesopore regime (>50 nm). This supports the fact that the pores of the aerogel are significantly larger than those of the xerogel (4 nm). Further discussion of the nitrogen adsorption of our reference catalysts can be found in references [13] and [16].

3.2.3 X-Ray Diffraction

The powder diffraction data of our prepared gels are shown in Fig. 3. Evidently, all aero- and xerogels exhibit non-Bragg diffraction up to the calcination temperature of 800 °C. Pure alumina aerogels have already transformed into crystalline γ-alumina at this temperature [16]. The observation that the gels stay amorphous is in accordance with the literature for non-sol–gel derived materials. For $LnAlO_3$ (with Ln=La, Pr and Nd) it is discussed that $LnAlO_3$ "barriers" form which suppress the formation of either pure Al_2O_3 or rare earth oxide domains [29, 30]. Yet, the exact mechanism of the stabilization is still discussed in the literature. The formation of larger $SmAlO_3$ domains is also observed for our catalyst but only after calcination at temperatures above 925 °C. Above 925 °C γ-Al_2O_3 also forms, but no Sm_2O_3 phases were detected. These temperatures, however, will not be reached under normal reaction conditions. Accordingly, it must be assumed that our xero- and aerogel catalysts either exhibit a homogenously mixed composition or consist of separated phases of alumina and samaria all of which are so small that non-Bragg diffraction dominates the XRD patterns.

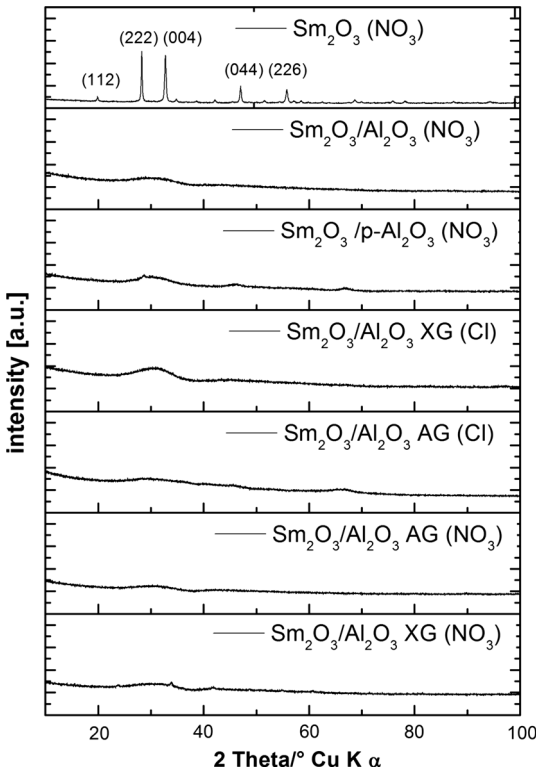

Fig. 3 X-Ray diffraction pattern of the sol–gel derived materials (aerogel [AG] and xerogel [XG]) and the reference catalysts (precursor used in the preparation is given in parenthesis). All samples were calcined at 800 °C before the XRD measurements were performed. Only the pure samarium oxide shows Bragg diffraction. The main reflections of cubic Sm_2O_3 are indicated by their (*hkl*). All other samples show only non-Bragg-scattering indicating that only very small crystalline areas are present in the sample

3.3 Catalysis

Results of the oxidative coupling of methane are summarized in Tables 2 and 3. Table 2 gives an overview on

Table 2 OCM reaction data for catalysts at 800 °C and a 4:1 CH_4:O_2 ratio

Catalyst[a]	Prep method—precursor[b]	$X(CH_4)$[c] (%)	$X^*(CH_4)$[d] (%)	$X(O_2)$[e] (%)	$S(C_2)$[f] (%)	$Y(C_2)$[g] (%)	SSA[h] (m^2/g)
10 mm ID tube							
Sm_2O_3	Calc. NO_3	22.3	17.7	100	48.5	8.6	3.5
Sm_2O_3/p-Al_2O_3	IWI-NO_3	21.8	17.0	100	35.7	6.1	78
Sm_2O_3/Al_2O_3	NO_3- NO_3	20.4	13.7	100	29.3	4.0	5.6
Al_2O_3 AG	NO_3	14.7	11.6	100	10.3	1.2	219
Al_2O_3 AG	Cl	17.2	12.8	100	22.4	2.9	236
Al_2O_3 XG	NO_3	19.8	14.1	100	18.8	2.6	189
Al_2O_3 XG	Cl	18.4	13.3	100	19.2	2.6	166
Sm_2O_3/Al_2O_3 AG	NO_3	16.6	14.3	100	23.3	3.3	164
Sm_2O_3/Al_2O_3 AG	Cl	18.2	13.8	100	31.6	4.4	120
Sm_2O_3/Al_2O_3 XG	NO_3	18.9	12.6	100	26.5	3.3	120
Sm_2O_3/Al_2O_3 XG	Cl	25.5	19.3	100	42.9	8.3	59
Flow study							
Sm_2O_3/Al_2O_3 XG[i]	Cl (120 sccm)	25.5	19.3	100	42.9	8.3	59
Sm_2O_3/Al_2O_3 XG	Cl (200 sccm)	25.3	19.6	100	46.1	9.0	59
Sm_2O_3/Al_2O_3 XG	Cl (280 sccm)	25.8	19.0	100	46.0	8.7	59
Sm_2O_3[i]	NO_3 (120 sccm)	22.3	17.7	100	48.5	8.6	3.5
Sm_2O_3	NO_3 (200 sccm)	23.1	18.6	100	44.5	8.3	3.5
Sm_2O_3	NO_3 (240 sccm)	23.3	18.8	100	43.4	8.2	3.5
4 mm ID tube							
75 mg Sm_2O_3/Al_2O_3 XG	Cl (80 sccm)	19.8	12.5	84.5	32.9	4.1	59
50 mg Sm_2O_3/Al_2O_3 XG	Cl (120 sccm)	12.1	8.5	48.9	33.9	2.9	59
10 mg Sm_2O_3–50 mg SiC	NO_3 (120 sccm)	12.6	9.7	50.7	42.3	4.1	

[a] Sm_2O_3/Al_2O_3 all have 20:80 Sm:Al atomic ratios (AG: aerogel and XG: xerogel)

[b] Preparation method: sol–gel method unless otherwise noted. *Calc.* calcination of NO_3 precursor. *IWI* incipient wetness impregnation. Precursors = NO_3 or Cl

[c] Methane conversion

[d] Methane conversion to C_2 and CO_x products

[e] Oxygen conversion

[g] C_2 product yield (calculated as $X^*(CH_4)\cdot S(C_2)\cdot 100$)

[f] C_2 product selectivity calculated according to Eq. 1

[h] *SSA* specific surface area m^2/g

[i] Duplicate entry to facilitate comparison

conversion, yield and selectivity to C_2 and CO_x while Table 3 shows the product distribution in more detail.

To benchmark the catalytic performance of our sol–gel derived materials, we prepared three different reference catalysts which are also based on alumina and samaria: (A) pure samaria was prepared from the calcination of samarium nitrate. This catalyst was used to evaluate if an alumina-supported catalyst—with less rare earth content—can be competitive with pure samaria. (B) A commercial porous alumina was impregnated with samarium nitrate and calcined. We chose this system to investigate potential differences in catalytic performance between our sol–gel system and porous catalysts with a less homogenous distribution of the catalytically active component. (C) Aluminum nitrate and samarium nitrate were dissolved in ethanol, dried and finally calcined (no gelation agent was added). In particular this last reference catalyst was prepared to evaluate if the additional synthetic effort of the sol–gel chemistry has a benefit for OCM. In addition, we prepared pure alumina aero- and xerogels to demonstrate that the addition of samarium is essential for appreciable C_2 yields.

For all our catalysts, we report two different methane conversions. The first one $X(CH_4)$ is based on the methane loss calculated from the difference between the initial concentration and the concentration of methane left in the product stream. The second one $X^*(CH_4)$ is calculated based on the yields of C_2 and CO_x products, i.e. the fraction

Table 3 Product distribution for gas-phase products with a CH_4:O_2 feed ratio of 4:1 at 800 °C

Catalyst[a]	Preparation method[b]	Product distribution [%]				C_2H_4/C_2H_6 ratio	CO_2/CO ratio
		C_2H_4	C_2H_6	CO_2	CO		
10 mm ID tube							
Sm_2O_3	NO_3	36.1	11.7	43.3	8.3	3.1	5.2
Sm_2O_3/p-Al_2O_3	IWI-NO_3	25.9	9.8	47.0	17.3	2.6	2.7
Sm_2O_3/Al_2O_3	NO_3-NO_3	22.1	7.2	38.2	32.5	3.1	1.2
Al_2O_3 AG	NO_3	2.3	7.9	54.8	34.9	0.3	1.6
Al_2O_3 AG	Cl	15.0	7.4	39.1	38.5	2.0	1.0
Al_2O_3 XG	NO_3	13.6	5.2	39.3	41.9	2.6	0.9
Al_2O_3 XG	Cl	13.2	6.0	39.8	41.0	2.2	1.0
Sm_2O_3/Al_2O_3 AG	NO_3	25.7	8.6	42.7	22.9	3.0	1.9
Sm_2O_3/Al_2O_3 AG	Cl	23.5	8.1	40.2	28.3	2.9	1.4
Sm_2O_3/Al_2O_3 XG	NO_3	18.8	7.7	37.1	36.5	2.4	1.0
Sm_2O_3/Al_2O_3 XG	Cl (120 sccm)	32.1	10.8	42.4	14.7	3.0	2.9
Flow Rate Study							
Sm_2O_3/Al_2O_3 XG	Cl (120 sccm)	32.1	10.8	42.4	14.7	3.0	2.9
Sm_2O_3/Al_2O_3 XG	Cl (200 sccm)	35.8	10.3	38.4	15.6	3.5	2.5
Sm_2O_3/Al_2O_3 XG	Cl (280 sccm)	36.1	9.9	36.2	17.8	3.6	2.0
Sm_2O_3	NO_3 (120 sccm)	36.1	11.7	43.3	8.3	3.1	5.2
Sm_2O_3	NO_3 (200 sccm)	32.8	11.8	45.4	10.0	2.8	4.5
Sm_2O_3	NO_3 (240 sccm)	32.0	11.0	45.5	11.1	2.9	4.1
4 mm ID tube							
75 mg Sm_2O_3/Al_2O_3 XG	Cl (80 sccm)	14.3	18.6	41.9	25.3	0.8	1.7
50 mg Sm_2O_3/Al_2O_3 XG	Cl (120 sccm)	11.7	22.1	34.9	31.3	0.5	1.1
10 mg Sm_2O_3–50 mg SiC	NO_3 (120 sccm)	15.3	27.0	43.9	13.8	0.6	3.2

[a] Sm_2O_3/Al_2O_3 all have 20:80 Sm:Al atomic ratios (AG: aerogel and XG: xerogel)

[b] Preparation method: sol–gel method unless otherwise noted. *Calc.* Calcination of NO_3 precursor. *IWI* incipient wetness impregnation. Precursors = NO_3 or Cl

of methane converted to C_2 and CO_x. Due to the chosen experimental conditions, the C_2H_4 yields are high in comparison to the yield of C_2H_6 and the yield of C_3H_8 was not significant in the current study. Although C_2H_4, which is produced via dehydrogenation of C_2H_6, is the more desired product of the C_2 fraction, this compound is also known to decompose easier and result in coking within the reactor [34]. The higher the difference between X(CH_4) and X*(CH_4), the presumably higher is the amount of C_2H_4 which is decomposed in the reactor (to coke via C_2H_2 formation) [35]. So we can assume that in case of large differences the originally formed C_2H_4 content is even higher. Within the following discussion, conversions are always based on X(CH_4), while for the C_2 selectivity (and yield) only the amount of methane converted to C_2 and CO_x is considered, i.e. X*(CH_4), as shown in Eq. 1.

$$S(C_2) = \frac{\text{sccm } CH_4 \text{ reacted to } C_2 \text{ products}}{\text{sccm } CH_4 \text{ reacted to } CO_x \text{ and } C_2 \text{ products}} \quad (1)$$

Within the group of reference catalysts, pure samaria shows the highest conversion of methane and also the highest C_2 selectivity (Table 2). The supported samaria on porous alumina (p-Al_2O_3) as well as the catalyst obtained from the metal nitrates show inferior performance. For both alumina-containing reference catalysts, a higher CO selectivity is observed in comparison to pure Sm_2O_3 (Table 3). In accordance with the high acidity of pure alumina, our pure alumina aero- and xerogels show the highest CO selectivity of all catalyst [36, 37]. The relatively high methane conversion of these samples is based on the fact that the number of strong acidic and basic sites of alumina is increased by dehydration at high temperatures [36].

Within the group of samaria–alumina gels, all aero- and xerogel catalysts, except the chloride derived Sm_2O_3/Al_2O_3 xerogel, exhibit similar methane conversions in the range of 16.5–19 %, which are comparable to the methane conversion obtained over the pure Al_2O_3 gels. Yet, the presence of samaria distinctly increases the C_2 selectivity (and lowers CO selectivity) in comparison to pure alumina. Nonetheless, compared to our supported reference catalysts, conversion and C_2 selectivity of most sol–gel systems

are inferior with one exception. The conversion and the C_2 selectivity of the chloride derived Sm_2O_3/Al_2O_3 xerogel catalyst are distinctly higher than the other aero- and xerogel catalysts, and quite similar to pure Sm_2O_3 (Table 2). Since the Sm_2O_3 content in the Sm_2O_3/Al_2O_3 xerogel is only 46 % by weight, versus 100 % for the pure Sm_2O_3 catalyst, the productivity per unit weight of Sm_2O_3 is higher over the Sm_2O_3/Al_2O_3 xerogel catalyst compared with the pure Sm_2O_3 catalyst.

Since it could be argued that experiments at O_2 conversions of 100 %, as reported above, are not suitable to judge the productivity of the catalysts in relation e.g. to the pure samaria reference catalyst, additional experiments were performed to probe the effects of O_2 conversion on these reactions. A significant portion of studies in the literature either report 100 % O_2 conversion or do not comment on the oxygen utilization [31–33]. The reason for this is that the methane conversion and C_{2+} productivity are maximized at 100 % O_2 conversion. However, it is also important to make sure that excess catalyst is not used as this would result in lower yields per gram of catalyst, and can also cause unwanted side reactions (in the unused part of the catalyst bed) which would further reduce the yields.

In the first series of experiments the total flow rate was increased sequentially for the best performing catalysts (Sm_2O_3/Al_2O_3–Cl–XG and the pure Sm_2O_3). However, with 400 mg of catalyst, the total flow rate could be more than doubled (to 280 sccm) without affecting the complete conversion of O_2, which suggests that there is excess catalyst in the reactor (Table 2). It is interesting to note that for the Sm_2O_3/Al_2O_3–Cl–XG catalyst the methane conversion and C_2 selectivity does not vary significantly even though the flow rate is increased from 120 to 280 sccm. In fact, it appears that the selectivity is increasing slightly (from 43 to 46 %) in the range from 120 to 200 sccm (Table 2), and the C_2H_4/C_2H_6 ratio also increases with flow rate (Table 3). Therefore, over this catalyst, the productivity (C_2 yield per unit time) can be increased significantly by increasing the flow rate without changing the fraction of methane converted to desired products. In contrast, it appears that the pure Sm_2O_3 exhibits a slight decrease in C_2 selectivity with increasing flow rate (from 48.5 to 43.5 %), which would increase the production of unwanted products. Therefore, at total flow rates of 200 sccm and above, the Sm_2O_3/Al_2O_3–Cl–XG catalyst outperforms the pure Sm_2O_3 catalyst, not only per unit weight of Sm_2O_3, but also per unit weight of catalyst.

As increasing the flow rate was not sufficient to obtain an oxygen conversion less than 100 %, a smaller amount of catalyst (50 mg) was loaded into the smaller diameter reactor (4-mm ID). At a total flow rate of 120 sccm an O_2 conversion of 49 % was observed for the Sm_2O_3/Al_2O_3–Cl–XG catalyst (Table 2). As can be seen in Table 2, the lower O_2 conversion is associated with a drastic decrease in both methane conversion and C_2 selectivity, and even at an O_2 conversion of 84.5 % the lower conversion and selectivity is apparent (see data for 75 mg and a flow rate of 80 sccm). Furthermore, the lower O_2 conversion is accompanied by considerably lower C_2H_4/C_2H_6 and CO_2/CO ratios (Table 3), and is therefore highly undesirable.

For pure Sm_2O_3 an O_2 conversion below 100 % could not be obtained with 50 or 25 mg of catalyst in the reactor. Reducing the amount of catalyst to 10 mg Sm_2O_3 and diluting with 50 mg of SiC in the reactor (to increase the bed length), the O_2 conversion was only 51 % at a flow rate of 120 sccm, which is almost the same as for the 50 mg Sm_2O_3/Al_2O_3–Cl–X.G (Table 2). Under these conditions the Sm_2O_3/Al_2O_3–Cl–XG catalyst exhibits a CH_4 conversion of 12.1 % at a C_2 selectivity of 34 % resulting in a C_2 yield of 2.9 %. The reference catalyst (pure Sm_2O_3), on the other hand, exhibited a CH_4 conversion of 12.6 % with a C_2 selectivity of 42 % giving rise to a C_2 yield of 4.1 %. Accordingly, the xerogel catalyst is less selective under these conditions, a fact that is not unexpected if it is taken into account that alumina is known to be a less favorable support as compared to a basic support, such as magnesia. Yet, under industrial applications, it is important to run at, or close to, 100 % O_2 conversion to maximize productivity. At 100 % O_2 conversion, the Cl-derived Sm_2O_3/Al_2O_3 xerogel can efficiently compete with the pure Sm_2O_3, as the yields are similar even though the amount of Sm_2O_3 in the reactor is lower for the xerogel. Furthermore, under conditions of 100 % O_2 conversion the xerogels demonstrate very stable selectivities and C_2 yields, and at higher flow rates they exhibit a superior behavior compared to the reference catalyst, which is important as the amount of C_2 actually produced is larger at the higher flow rates.

A beneficial effect of chloride for OCM has already been discussed for the OCM reaction as the oxidation of ethane to CO_x is suppressed [38, 39]. While we were not able to detect chlorine residues within our chloride derived xerogel after calcination of the material, it is possible that a trace amount could be present in the catalysts or on the catalyst surface. Furthermore, it can be assumed that the removal of chlorine between 700 and 800 °C is connected with a rearrangement of the surface possibly leading to different active sites. In addition, chloride is known to enhance atom mobility within catalysts [40]. An explanation based on such an effect is also corroborated by the fact that the xerogel from chloride shows a SSA which is smaller by a factor of 2–3 in comparison to the other sol–gel derived catalysts. However the mere reduction of the SSA cannot be the reason for the better performance of the catalyst alone, otherwise especially the reference catalyst on the basis of aluminum and samarium nitrate with only one tenth of the SSA should outperform the xerogel.

An unambiguous interpretation of the enhanced catalytic activity is not straightforward. In case of alumina supported samaria catalysts, Capitán et al. reported that the catalytic activity is a delicate function of the morphology and the surface composition [15]. Clearly, further studies are necessary to investigate this aspect in more detail. However, the current study reveals that Sm_2O_3/Al_2O_3 sol–gel prepared catalysts can compete with a pure Sm_2O_3 catalyst, which indicates that Al_2O_3 can be considered as a viable support in the oxidative coupling of methane. Furthermore, from a practical point of view, our study shows that the EAM method is rather versatile with respect to precursors and processing conditions but that the resulting catalytic properties can vary to some degree. This is of course in agreement with impregnated catalysts where the catalytic properties can also depend drastically on the preparation conditions, e.g. on the precursor used.

3.4 Coating of the Catalyst

Aiming at decreasing the samaria content and optimizing the overall flow pattern as discussed in the introduction, the use of gel coatings applied to suitable monoliths (ideally macroporous ceramic open cell foams [23, 24]) is the next logical step. Following this rationale we started first experiments trying to use EAM for the preparation of highly active catalytic coatings, i.e. the deposition of a thin layer of our Sm/AlO_x catalyst onto a catalytically inert substrate. For a first test demonstrating the general applicability, we chose a flat SiO_2 substrate facilitating the microscopic characterization by SEM. Figure 4 shows a micrograph of the coated surface of SiO_2 after calcination at 800 °C. The obtained xerogel film is clearly mesoporous (18–30 nm) and free of cracks. This is in accordance with the results of pore size distribution from BJH analysis of the non-coated xerogel. Note that the initial low viscosity of the sol allows also the coating of more tortuous structures such as mesoporous alumina or ceramic foams. This renders the coating approach rather flexible.

4 Conclusions

In this report, we describe a new sol–gel synthesis route for samaria catalysts which are embedded in an alumina matrix. The preparation follows an approach that has previously been described for pure rare earth oxides and has been extended to mixed oxides. It is based on the so-called epoxide addition method having the advantage that instead of expensive alkoxides simple chloride or nitrate salts can be used. The resulting aero- and xerogels are mesoporous with the supercritically dried aerogels exhibiting a higher porosity than the air-dried xerogels which undergo shrinkage due to capillary forces during solvent evaporation. In contrast to pure alumina or samaria aero/xerogels, the mixed systems stay amorphous even after calcination to 800 °C. EF-TEM images reveal an intimate mixing of Al and Sm on the nanoscale, meaning that the materials either consist of a homogeneously mixed oxide phase or of very small domains which cannot be resolved.

Within the present work, the suitability of the aerogels and xerogels as catalysts for the oxidative coupling of methane (OCM) was tested. All systems performed better in the reaction than pure alumina aero- and xerogels. In comparison to pure samaria, the xerogel derived from chlorides showed a good performance with comparable C_2 yields under conditions of 100 % oxygen conversion. This result demonstrates that embedding the samaria in a matrix of cheap alumina is a suitable strategy to disperse the samaria. Notably, the performance is superior to the impregnated samaria catalyst (exhibiting a similar surface area), revealing that the sol–gel approach can be the more beneficial strategy to disperse the catalytically active

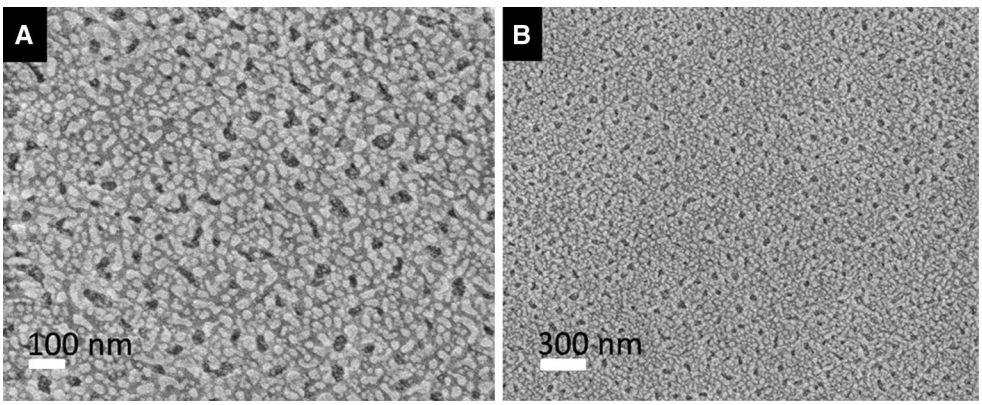

Fig. 4 SEM images of a flat silicia support which is coated with a thin layer of our Al_2O_3/Sm_2O_3 xerogel from chloride after calcination at 800 °C. The coating is homogenous, free of cracks and is clearly mesoporous

component in comparison to a classical deposition techniques, such as impregnation.

In addition to the preparation of aerogel and xerogel particles, the EAM synthesis also allows the fabrication of xerogel films which can be coated on a suitable (monolithic) support. First results for such films coated on a silica support prove that films can be obtained which are mesoporous and free of cracks.

Acknowledgements We thank Prof. Th. Gesing and Dr. J. Birkenstock (University Bremen) for assistance with the XRD experiments and Dr. Karsten Thiel (Fraunhofer Institute IFAM, Bremen) and Dr. Volkmar Zielasek (University Bremen) for TEM measurements. We also gratefully acknowledge financial support for this work provided by the Deutsche Forschungsgemeinschaft (DFG) through Grant number BA1710/19-1 and the National Science Foundation, Division of Chemistry, through Grant number 1026712. BN is grateful for a stipend of the Deutsche Telekom Stiftung. TE is grateful for a graduate student fellowship from the University of Florida.

References

1. Bundesanstalt für Geowissenschaften und Rohstoffe (2012) Reserves, Resources and Availability of Energy Resources
2. Holmen A (2009) Catal Today 142:2–8
3. Lunsford JH (1995) Angew Chem Int Ed 34:970–980
4. Choudhary V (1991) J Catal 130:411–422
5. Ito T, Lunsford JH (1985) Nature 314:721–722
6. Jiang ZC, Yu CJ, Fang XP (1993) S.B., Li, H.L. Wang. J Phys Chem 97:12870–12875
7. Arndt S, Otremba T, Simon U, Yildiz M, Schubert H, Schomäcker R (2012) Appl Catal A 425–426:53–61
8. Arndt S, Simon U, Heitz S, Berthold A, Beck B, Görke O, Epping J-D, Otremba T, Aksu Y, Irran E, Laugel G, Driess M, Schubert H, Schomäcker R (2011) Top Catal 54:1266–1285
9. Elkins TW, Neumann B, Bäumer M, Hagelin-Weaver HE (2014) ACS Catal 4:1972–1990
10. Otsuka K, Jinno K, Morikawa A (1986) J Catal 100:353–359
11. Forlani O, Rossini S (1992) Mater Chem Phys 31:155–158
12. Otsuka K, Inno K (1985) Chem Lett 144:499–500
13. Elkins TW, Hagelin-Weaver HE (2013) Appl Catal A 454:100–114
14. Vereshchagin SN, Ross JRH (1995) Catal Today 24:285–287
15. Capitán MJ, Malet P, Centeno MA, Munoz-Paez A, Carrizosa I, Odriozola JA (1993) J Phys Chem 97:9233–9240
16. Baumann TF, Gash AE, Chinn SC, Sawvel AM, Maxwell RS, Satcher JH (2005) Chem Mater 17:395–401
17. Tokudome Y, Nakanishi K, Kanamori K, Fujita K, Akamatsu H, Hanada T (2009) J Colloid Interface Sci 338:506–513
18. Debecker DP, Mutin PH (2012) Chem Soc Rev 41:3624–3650
19. Gash AE, Tillotson TM, Satcher JH, Poco JF, Hrubesh LW, Simpson RL (2001) Chem Mater 13:999–1007
20. Koebel MM, Nadargi DY, Jimenez-Cadena G, Romanyuk YE (2012) ACS Appl Mater Interfaces 4:2464–2473
21. Aigler JM, Lunsford JH (1991) Appl Catal 70:29–42
22. Wang W, Ji S, Pan D, Li C (2011) Fuel Process Technol 92:541–546
23. Liu H, Yang D, Gao R, Chen L, Zhang S, Wang X (2008) Catal Commun 9:1302–1306
24. Neumann B, Elkins TW, Dreher W, Hagelin-Weaver H, Nino JC, Bäumer M (2013) Catal Sci Technol 3:89–93
25. Bytyn W, Baerns M (1986) Appl Catal 28:199–207
26. Rane VH, Chaudhari ST, Choudhary VR (2008) J Nat Gas Chem 17:313–320
27. Choudhary VR, Rane VH, Chaudhari ST (1997) Appl Catal A 158:121–136
28. Clapsaddle BJ, Neumann B, Wittstock A, Sprehn DW, Gash AE, Satcher JH, Simpson RL, Bäumer M (2012) J Sol–gel Sci Technol 64:381–389
29. Oudet F (1988) J Catal 114:112–120
30. Schaper H, Doesburg EBM, Van Reijen LL (1983) Appl Catal 7:211–220
31. Spinicci R, Marini P, De Rossi S, Faticanti M, Porta P (2001) J Mol Catal A 176:253–265
32. Baidya T, van Vegten N, Verel R, Jiang Y, Yulikov M, Kohn T, Jeschke G, Baiker A (2011) J Catal 281:241–253
33. Ferreira VJ, Tavares P, Figueiredo JL, Faria JL (2013) Catal Commun 42:50–53
34. Taniewski M, Lachowicz A, Lachowicz R, Czechowicz D, Skutil K (1994) Ind Eng Chem Res 33:185–190
35. Towell GD, Martin JJ (1961) AlChE Journal 7:693–696
36. Wischert R, Copéret C, Delbecq F, Sautet P (2011) Angew Chem 123:3260–3263
37. Martin GA, Mirodatos C (1995) Fuel Process Technol 42:179–215
38. Burch R, Chalker S, Loader P, Rice DA, Webb G (1991) Appl Catal A 79:265–279
39. Burch R, Chalker S, Loader P, Thomas JM, Ueda W (1992) Appl Catal A 82:77–90
40. Bartholomew CH (2001) Appl Catal A 212:17–60